Measurement of electron-impact ionization cross sections for hydrogenlike high-Z ions

R. E. Marrs, S. R. Elliott,* and J. H. Scofield
Lawrence Livermore National Laboratory, Livermore, California 94551
(Received 12 December 1996)

Electron-impact ionization cross sections have been measured for the hydrogenlike ions of molybdenum, dysprosium, gold, and bismuth at selected electron energies between 1.3 and 3.9 times threshold. The cross sections were obtained from x-ray measurements of the equilibrium ionization balance in an electron beam ion trap. The measured cross sections agree with recent relativistic distorted-wave calculations that include both the Moeller interaction and exchange. [S1050-2947(97)03408-2]

PACS number(s): 34.80.Kw, 32.30.Rj

I. INTRODUCTION

Electron-impact ionization is a key process in the physics of highly charged high-Z ions, and accurate values for high-Z ionization cross sections are required for a complete understanding of electron-ion collisions. In addition to its fundamental role in basic atomic collision physics, electron-impact ionization also has a practical application in high-temperature plasmas and highly-charged-ion sources, where it is the process by which highly charged ions are usually produced. Unfortunately, there are very few measurements of ionization cross sections for highly charged ions, and almost none at all for the highest charge states. There is a long history of theoretical calculations of electron-impact ionization cross sections, ranging from simple semiempirical formulas to sophisticated relativistic distorted-wave calculations. The calculations are not easy due to the presence of two electrons in the final state, and different types of calculations often produce very different cross-section values.

The hydrogenlike isoelectronic sequence of one-electron ions is the simplest system for studying ionization cross sections because multielectron effects are completely absent and only direct single-electron-impact ionization contributes to the cross section. For example, excitation autoionization does not occur for hydrogenlike target ions. Although the atomic system is very simple, there are nevertheless discrepant theoretical calculations of ionization cross sections for hydrogenlike ions, particularly at high electron energy where the ionization cross sections are sensitive to relativistic interactions [1–4]. Differences among recent fully relativistic distorted-wave calculations can be attributed to the choice of electron-electron interaction. For example, the inclusion of lowest-order QED terms and exchange amplitudes was recently found to have a significant effect on the cross sections at high electron energy [3,4].

Other than our previous measurement of the ionization cross section for hydrogenlike U^{91+} [5], there have been no direct measurements of the electron-impact ionization cross sections for very highly charged ions. For lower charge states and electron energies, ionization cross sections have been measured in crossed- and merged-beam experiments [6,7]. In another type of experiment, the evolution of the ionization balance in an electron-beam ion source was used to obtain ionization cross sections [8]. Ionization cross sections for several lithiumlike ions have been measured in an electron-beam ion trap (EBIT) by comparing the rates of ionization and dielectronic recombination [9]. Very-highly-charged ions can be produced by stripping relativistic accelerator beams in foil targets, but their electron-impact ionization cross sections are too small to measure with a crossed or merged electron beam. However, measurements of the stripping of relativistic beams of highly charged uranium ions channeled in crystal targets have been used to infer electron-impact ionization cross sections [10].

Here we report the results of ionization cross-section measurements for the hydrogenlike ions of molybdenum, dysprosium, gold, and bismuth at selected electron energies between 1.3 and 3.9 times threshold. We have previously published one other result using the same technique, a measurement of the ionization cross section of hydrogenlike uranium [5]. Taken together, these results form a sufficiently complete set of measurements to distinguish among different theoretical models and determine reliable K-shell ionization cross sections for all heavy elements.

II. EXPERIMENTAL METHOD

Hydrogenlike ions were produced and trapped in the high-energy electron beam ion trap (Super EBIT) at the Lawrence Livermore National Laboratory [11]. Ions in an EBIT are continuously exposed to the electron beam in which they are trapped, resulting in an easily observed x-ray emission spectrum. We use radiative recombination (RR) x-ray lines from K-shell capture to determine the relative abundance of hydrogenlike and bare ions, the presence of which is a measure of the hydrogenlike ionization cross section. The relative rates of ionization and recombination of the trapped ions determine the equilibrium ionization balance in a manner analogous to chemical equilibrium. The predominant recombination process is RR. Dielectronic recombination, a resonant process, does not contribute at the electron energies used here, and three-body recombination is negligible. (A small but necessary correction for charge-exchange recombination with neutral gas atoms will be explained later.) Thus, for hydrogenlike and bare ions, the relationship between the cross sections and abundances at equilibrium is

*Present address: Department of Physics, University of Washington, Seattle, WA 98195.

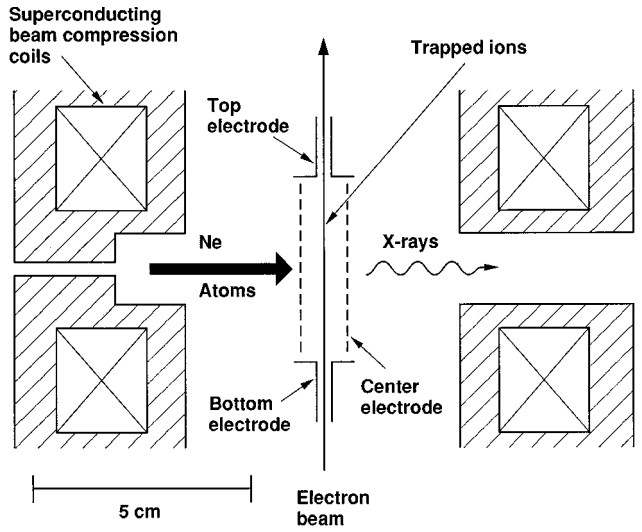

FIG. 1. Trap configuration. The cylindrical center electrode is slotted to facilitate x-ray emission and neon cooling gas injection.

$$\frac{N_{\rm bare}}{N_{\rm H}} = \frac{\sigma^{\rm ion}_{\rm H\rightarrow bare}}{\sigma^{\rm RR}_{\rm bare\rightarrow H}}, \tag{1}$$

where $N_{\rm bare}$ and $N_{\rm H}$ are the abundances of the bare and hydrogenlike charge states. The cross sections for radiative recombination and ionization are given in obvious notation.

The hydrogenlike ionization cross section $\sigma^{\rm ion}_{\rm H\rightarrow bare}$ can be obtained from Eq. (1) if the other quantities are known. We obtained RR cross sections from theoretical calculations [12]. Calculated RR cross sections provide a convenient and accurate normalization for EBIT cross section measurements. The RR calculation is basically the same as that for the inverse process of photoionization, for which there is an extensive database of measured cross sections. For the elements and photon energies used in the present work, calculated and measured photoionization cross sections agree to within the experimental uncertainties of typically 3% [13], so we take $\pm 3\%$ as the uncertainty in our theoretical RR cross sections. The RR process is particularly simple for bare target ions as it involves a single electron radiating in the field of the nucleus. References for the relativistic treatment of RR used in the present calculations can be found in Ref. [12] and in the review article by Pratt *et al.* [14]. In our calculations the finite nuclear size was taken into account in the potential seen by the electron, and all significant partial waves and radiation multipoles were included. In the 100-keV energy range radiation multipoles up to order 10 contribute at the 0.1% level.

A. Production of high-*Z* hydrogenlike ions

The EBIT was developed for x-ray measurements of trapped highly charged ions [15]. Detailed descriptions of the apparatus can be found elsewhere [11,16]. A diagram of the trap portion of the apparatus showing the features relevant to the present work is shown in Fig. 1. The electron beam is compressed to high density ($\sim$5000 A/cm^2) and guided along the axis of the trap by a 3-T magnetic field produced by superconducting coils. Ions are trapped radially by the negative space charge potential of the electron beam. Axial confinement is achieved by bias voltages applied to three drift tubes (i.e., trap electrodes). Collisions with beam electrons strip the ions to high charge states and produce x-ray emission that is observed at 90° to the electron beam in the midplane of the trap.

Highly charged ions trapped in an electron beam are heated by small-angle Coulomb collisions with beam electrons. A comparison of rates shows that, in the absence of a cooling mechanism, ions will ''evaporate'' from the beam before reaching high charge states. We use an evaporative ion-ion cooling technique employing a mixture of low-charge and high-charge ions to remove the heat from electron beam heating [5,17]. In the present work, the low-charge cooling ions were introduced from a collimated beam of neon gas atoms that intersected the electron beam at 90° as shown in Fig. 1. A schematic of the gas injector geometry is shown in Fig. 2. Some of the neon atoms are ionized by the electron beam and captured in the trap. The (low-charge) neon ions are then heated by collisions with hotter high-*Z* ions before escaping axially (evaporating) from the trap with the removal of energy. Evaporative cooling is extremely effective, and for every element studied here we obtained a population of cool high-*Z* ions that remained trapped for several minutes, a time much longer than the equilibration time for the ionization balance.

B. X-ray measurements

The elements studied in the present work were injected into the Super EBIT trap as low-charge-state ions from a

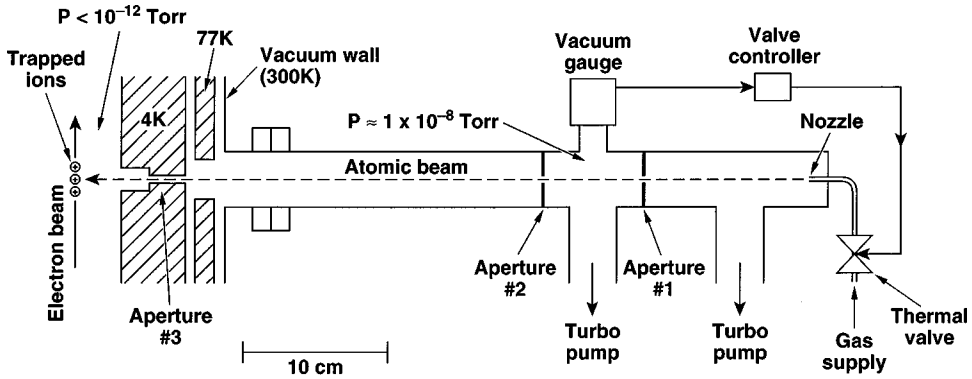

FIG. 2. Layout of the neon gas injection system. Apertures 1 and 2 have a diameter of 4.6 mm, and aperture 3 has a diameter of 3.1 mm. The nozzle inside diameter is 1.5 mm. The thermal valve is regulated to maintain a constant pressure in the region between apertures 1 and 2.

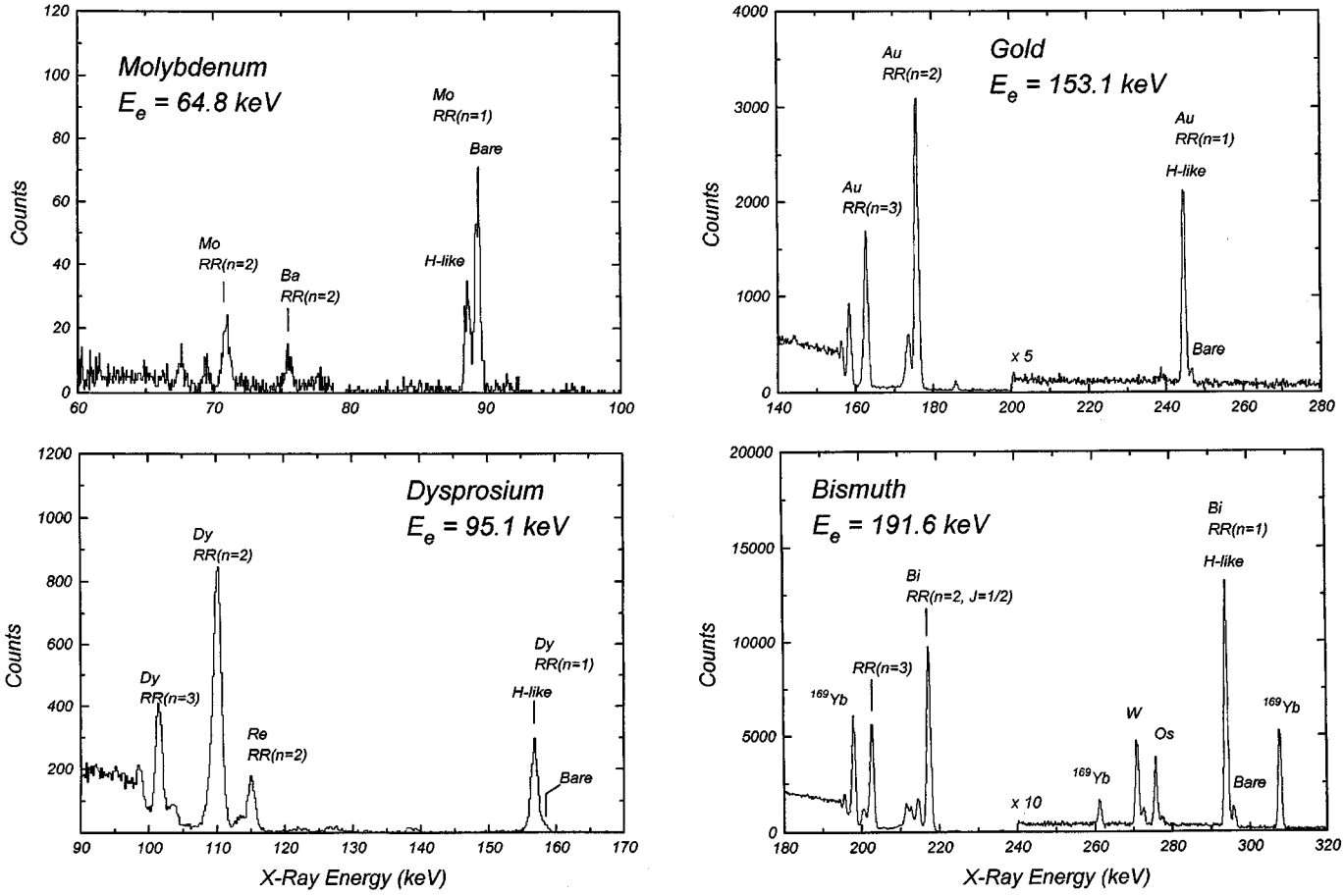

FIG. 3. Typical radiative-recombination x-ray spectra for each of the four elements studied. Peaks labeled with the chemical symbols of other elements are due to contaminant ions. The molybdenum spectrum was obtained with a 1-cm-thick planar germanium detector, and the other spectra were obtained with a 3-cm-thick coaxial germanium detector. The lines labeled ^{169}Yb in the bismuth spectrum are from a radioactive source used for energy calibration. The high-energy portions of the gold and bismuth spectra have been multiplied by factors of 5 and 10, respectively, for display purposes.

vacuum spark source [18]. Immediately before injection, any ions already present in the trap were dumped by removing the axial trap potential. When the ion source was triggered, the axial trap potential was pulsed up in order to capture some of the ions from the source. Once trapped, the ions lose their outer electrons very quickly, and the hydrogenlike ionization stage is reached within a few seconds or less, depending on the element and electron energy used. After a preset delay following ion injection that ranged from 5 to 7 s, x-ray spectra were accumulated for a 14-s period for the three lightest elements and a 35-s period for bismuth. This dump-inject-count cycle was repeated many times until a sufficient number of counts was accumulated in the RR($n=1$) x-ray lines. The number of ions retained in the trap after injection is determined by the evaporative cooling power and is very reproducible from cycle to cycle. We estimate that roughly 10% of the electron-beam space charge was neutralized by ion charges for the conditions used in the present cross-section measurements.

Planar (for molybdenum) and coaxial (for the other elements) germanium detectors were used to obtain RR x-ray spectra. We were able to measure ionization cross sections at four different electron energies for hydrogenlike molybdenum. For the heavier elements the electron energy range was limited on the high side by the ~200-keV maximum energy of our Super EBIT, and on the low side by the small size (and therefore small bare-ion abundance) of the ionization cross sections near threshold, so fewer electron energies were used. A typical x-ray spectrum for each element is shown in Fig. 3. A complete list of the electron energies used appears in Table I. The electron energies were determined from the observed energies of the RR lines and have an uncertainty of approximately 0.2 keV, an energy range over which the change in the ionization and RR cross sections is not significant.

The observed x-ray spectra consist of a series of peaks corresponding to RR into the open shells of the highly stripped target ions. RR into the higher Rydberg levels joins smoothly with bremsstrahlung radiation at an x-ray energy equal to the electron beam energy. X-ray emission from RR into the partially filled inner shells reveals information about the ion charge-state distribution. X-ray emission from RR into the empty higher Rydberg levels is insensitive to small changes in the charge-state distribution and provides a measure of the total number of ions in the electron beam. RR into the K shell of bare and hydrogenlike target ions produces a barely resolved doublet of lines from which we determine the relative abundance of bare and hydrogenlike ions. The RR spectra were fitted with a line shape consisting of a Gaussian peak plus a shelf on the low-energy side. Separate

TABLE I. Ionization cross sections for hydrogenlike ions. Threshold energies (i.e., ionization potentials) are given in the second column. The third and fourth columns give the incident electron energy in keV and threshold units, respectively. The quantities $\sigma^{RR}_{bare\to H}$ and $\langle\sigma^{CX}_{bare}\rangle$ are the total RR and effective charge-exchange recombination cross sections as explained in the text. The last four columns are ionization cross sections. The relativistic distorted wave calculations are from Moores and Reed Ref. [4]. Cross section units are 10^{-24} cm^2.

Element (Z)	H-like I. P. (keV)	E_e (keV)	E_e/I.P.	$\sigma^{RR}_{bare\to H}$	$\langle\sigma^{CX}_{bare}\rangle$	Present Experiment	Rel. D.W. with Breit	Rel. D.W.	Lotz
Mo (42)	24.6	31.5	1.28	90.33	7.2	15.9 ±1.6	15.1	14.8	14.3
		36.1	1.47	72.39	7.0	21.2 ±1.9	20.8	20.0	19.4
		64.8	2.63	26.56	3.1	30.8 ±2.6	31.6	29.9	27.3
		95.6	3.89	13.01	7.3	34.7 ±7.2	32.2	30.2	25.9
Dy (66)	63.1	95.1	1.51	67.2	6.6	4.17±0.58	4.13	3.47	3.1
		153.1	2.43	30.2	6.6	6.29±0.83	6.11	5.06	4.1
Au (79)	93.3	153.1	1.64	58.6	9.6	2.33±0.33	2.47	1.91	1.6
Bi (83)	104.1	191.6	1.84	48.5	7.7	2.37±0.19	2.40	1.76	1.4
U (92)	131.8	198	1.50	67.5	7.5	1.55±0.27[a]	1.44	0.93	0.7

[a]Value taken from Ref. [5].

fits to high-statistics lines from radioactive sources confirmed the accuracy of this line shape for our detectors. The separation of the two members of the RR($n=1$) doublet was frozen at the theoretical value during the fitting procedure, and their widths were constrained to be the same. The electron-beam energy spread is roughly ten times less than the detector resolution, so its contribution to the line shape (which would be roughly Gaussian and the same for all RR peaks) is hidden in the fitted line width. The differential RR cross section at 90° for K-shell capture differs by a factor of 2 for bare and hydrogenlike target ions, as expected from the number of K-shell vacancies, so the abundance ratio of bare and hydrogenlike target ions was obtained by adjusting the fitted RR($n=1$) peak areas by a factor of 2. (The theoretical RR ratio calculated with our relativistic code differs from 2 by less than 1%.)

C. Approach to equilibrium

The abundance of each ion charge state in the trap is coupled to that of the adjacent charge states by charge-changing collisions. The rate of change of the abundance of a bare ion N_{bare} is

$$\frac{dN_{bare}}{dt}=N_H(j_e/e)\sigma^{ion}_{H\to bare}-N_{bare}[(j_e/e)\sigma^{RR}_{bare\to H}+n_0 v\,\sigma^{CX}_{bare}], \quad (2)$$

where N_H is the abundance of hydrogenlike ions, j_e is the effective electron current density, and e is the electron charge. The cross sections for electron-impact ionization, RR, and charge-exchange recombination with neutral gas are denoted by $\sigma^{ion}_{H\to bare}$, $\sigma^{RR}_{bare\to H}$, and σ^{CX}_{bare}, respectively. In the charge-exchange term, n_0 is the neutral gas density and v is the ion neutral collision velocity (approximately the ion thermal velocity). The charge-exchange cross section includes both single and multiple electron capture. For hydrogenlike ions the corresponding equation is

$$\frac{dN_H}{dt}=N_{He}(j_e/e)\sigma^{ion}_{He\to H}-N_H[(j_e/e)\sigma^{RR}_{H\to He}+n_0 v\,\sigma^{CX}_H+(j_e/e)\sigma^{ion}_{H\to bare}]+N_{bare}[(j_e/e)\sigma^{RR}_{bare\to H}+n_0 v\,\sigma^{CX}_{bare\to H}]. \quad (3)$$

Similar equations may be written for the other ionization stages, resulting in a set of coupled differential equations for the complete ionization balance. We are interested only in the (relative) abundance of bare and hydrogenlike ions at or near the equilibrium ionization balance. These two ionization stages are coupled to each other through Eq. (2), which reduces to the simple relationship of Eq. (1) if we assume that the ionization balance is in equilibrium (i.e., $dN_{bare}/dt=0$) and neglect charge-exchange recombination.

Although we are interested only in the steady-state ionization balance, an estimate of the rates for the relevant collision processes is helpful for understanding how rapidly equilibrium is achieved. The rate constant λ for an electron-ion collision process in an EBIT is given by:

$$\lambda=(j_e/e)\sigma, \quad (4)$$

where σ is the cross section for the collision process. The effective current density j_e accounts for the overlap of the ions and the electron beam. For the shallow axial trap depths (typically 10 V) and low ion temperatures used here the overlap factor is approximately one, so we estimate that $j_e \sim 5000$ A/cm^2 for the ~180-mA beam currents used for most of the present measurements. (Some of the molybdenum data were taken at an 80-mA beam current, and j_e was proportionately smaller.)

Rewriting Eq. (2) in terms of rate constants, we have

$$\frac{dN_{bare}}{dt}=N_H\lambda^{ion}_H-N_{bare}[\lambda^{RR}_{bare}+\lambda^{CX}_{bare}]. \quad (5)$$

The solution to Eq. (5) for a hydrogenlike bare ionization balance that is initially out of equilibrium (i.e., with $N_{\rm bare}$ initially depleted) has the form

$$N_{\rm bare}=N_{\rm bare}^{\rm equil}(1-e^{-\lambda_{\rm bare}t}), \tag{6}$$

where $\lambda_{\rm bare}=\lambda_{\rm H}^{\rm ion}+\lambda_{\rm bare}^{\rm RR}+\lambda_{\rm bare}^{\rm CX}$ and $N_{\rm bare}^{\rm equil}$ is the equilibrium abundance of bare ions. (For this estimate we have neglected the feeding of $N_{\rm H}$ from other ionization stages and assumed that $N_{\rm bare}+N_{\rm H}$ is constant.)

As can be seen from Eq. (6), the abundance ratio of hydrogenlike and bare ions approaches equilibrium with a rate given by $\lambda_{\rm bare}$. Even for very small ionization cross sections, equilibrium is achieved quickly because of the fast RR rate. (See Table I for a list of the cross sections.) For the present measurements $\lambda_{\rm bare}$ ranges from 0.8 to 3.5 s^{-1}. Both the estimated time to reach the hydrogenlike ionization stage and the hydrogenlike bare equilibration time $(\lambda_{\rm bare})^{-1}$ are in all cases much smaller than the delay time between the trapping of ions and the start of data acquisition, so we expect the ionization balance to be solidly in equilibrium during data acquisition. The acquired x-ray spectra were nevertheless routed into seven different time bins of equal length and examined for changes in the ionization balance. None were found, and the seven spectra were summed together for further analysis.

For the elements studied in the present work, the seven time-routed spectra show a gradual decline in the total x-ray count rate of roughly 1% per second due to a slow loss of ions from the trap. The corresponding rate coefficient is $\lambda^{\rm loss}\approx 0.01\ s^{-1}$, which is two orders of magnitude smaller than $\lambda_{\rm bare}$, the equilibration rate for the hydrogenlike bare ionization balance.

D. Charge-exchange recombination

As explained above, it is necessary to inject neutral gas into our trap in order to supply light ions for the evaporative cooling process. This affects the ionization balance of the highly charged ions through charge-exchange recombination. Neither the charge-exchange recombination cross section nor the absolute neutral density in our trap is known. However, the neutral neon density can be varied by known factors by adjusting the flow rate in the neon gas injector. We correct for charge-exchange recombination by running at several different neutral densities and extrapolating the effect to zero. It is not possible to measure cross sections at near-zero neutral density because the number of trapped ions is small and the count rate is too low. We assume that the increment in the gas-injector pressure gauge reading above background is proportional to the density of neutral neon injected into the trap. The location of the pressure gauge is shown in Fig. 2. It responds to gas skimmed by the second of three collimating apertures.

1. Effect on ionization cross sections

To account for charge-exchange recombination, Eq. (1) must be modified with the addition of another term. The correct equation for the hydrogenlike ionization cross section is

$$\sigma_{\rm H\to bare}^{\rm ion}=\frac{N_{\rm bare}}{N_{\rm H}}(\sigma_{\rm bare\to H}^{\rm RR}+\langle\sigma_{\rm bare}^{\rm CX}\rangle). \tag{7}$$

Equation (7) follows from Eq. (2) if $dN_{\rm bare}/dt$ is set equal to zero. Here $\langle\sigma_{\rm bare}^{\rm CX}\rangle$ is a density-dependent effective charge-exchange recombination cross section given by $\langle\sigma_{\rm bare}^{\rm CX}\rangle=(e/j_e)n_0 v\,\sigma_{\rm bare}^{\rm CX}$. The dimensionless quantity $(e/j_e)n_0 v$ is much less than one, and $\langle\sigma_{\rm bare}^{\rm CX}\rangle$ is smaller than $\sigma_{\rm bare\to H}^{\rm RR}$ for all of the present measurements. We used Eq. (7) to obtain all of the hydrogenlike ionization cross sections reported in the present work, with values for $\langle\sigma_{\rm bare}^{\rm CX}\rangle$ and $\sigma_{\rm bare\to H}^{\rm RR}$ as given in Table I.

2. Extrapolation to zero neutral density

Since all of the measurements reported here and in Ref. [5] were performed under similar conditions, we expect $\langle\sigma_{\rm bare}^{\rm CX}\rangle$ to have similar values in all cases. However, we determined $\langle\sigma_{\rm bare}^{\rm CX}\rangle$ separately for each element using an extrapolation procedure that differs slightly for the different elements studied. For molybdenum, the ratio of K-shell RR x-ray intensities for hydrogenlike and bare target ions, $I_{\rm H}^{\rm RR}/I_{\rm bare}^{\rm RR}$, was measured for several different neon gas densities at one of the electron beam energies (64.8 keV). This ratio is equal to $\frac{1}{2}$ the abundance ratio of hydrogenlike and bare ions. So, rearranging Eq. (7), we expect

$$\frac{I_{\rm H}^{\rm RR}}{I_{\rm bare}^{\rm RR}}=\tfrac{1}{2}\frac{N_{\rm H}}{N_{\rm bare}}=\tfrac{1}{2}(1/\sigma_{\rm H\to bare}^{\rm ion})\left(\sigma_{\rm bare\to H}^{\rm RR}+\frac{K_{\rm Ne}n_{\rm Ne}}{j_e}\right), \tag{8}$$

where $K_{\rm Ne}$ is a constant and $n_{\rm Ne}$ is the density of neutral neon atoms. The second term is the effective charge-exchange recombination cross section $\langle\sigma_{\rm bare}^{\rm CX}\rangle$ rewritten to show the linear dependence on neon density. The neglect of the small ion loss rate $\lambda^{\rm loss}$ is justified even at very low cooling gas density because our time-dependent data show that it is essentially unaffected by the neutral density and is always roughly two orders of magnitude smaller than the other rates. The number of ions lost from the trap immediately ($\sim$100 ms) after injection during thermal equilibration of the ions is of course strongly dependent on neutral gas density.

Figure 4 shows the measurements of $I_{\rm H}^{\rm RR}/I_{\rm bare}^{\rm RR}$ for molybdenum as a function of neon density. The dashed line is a best guess at the true density dependence; its slope, and the fact that $\langle\sigma_{\rm bare}^{\rm CX}\rangle$ must be zero at zero neutral density, were used to determine the value of $\langle\sigma_{\rm bare}^{\rm CX}\rangle$ as a function of neon density. Ionization cross sections for hydrogenlike molybdenum were determined at four different electron-beam energies from data runs at neutral densities ranging from 0.2 to 1.0 on the scale of Fig. 4. The values of $\langle\sigma_{\rm bare}^{\rm CX}\rangle$ used are listed in Table I.

3. Background gas

The trapped ions in our apparatus are almost completely surrounded by electrodes and x-ray windows at a temperature of 4 K, and the density of background (not neon) gas is extremely low. However, background gas also contributes to charge-exchange recombination, and its presence would appear as an unrecognized offset in the pressure scale of Fig. 4.

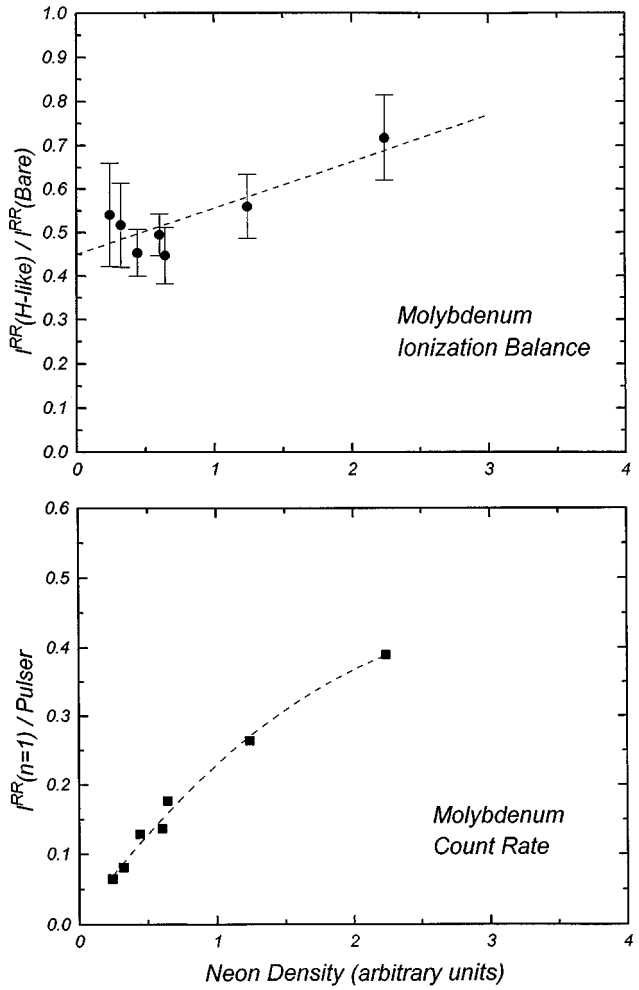

FIG. 4. Effect of neutral neon density on the ionization balance and number of trapped molybdenum ions at 64.8-keV electron energy. Top: the ratio of hydrogenlike to bare ions as indicated by the RR intensities. The dashed curve is a best guess at the true density dependence. Bottom: total x-ray count rate for RR into the K shell (normalized to a repetitive pulser). Statistical uncertainties are roughly the size of the plotted points. The dashed curve is to guide the eye.

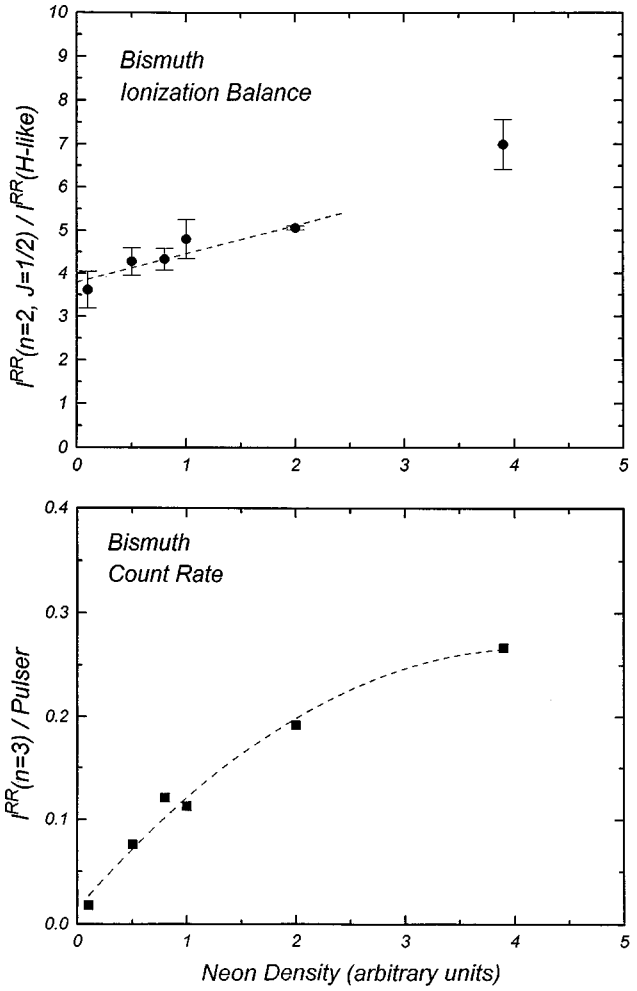

FIG. 5. Similar to Fig. 4 but for bismuth at 191.6-keV electron energy. The point with the small error bar at a density of approximately 2 comes from a long high-statistics run used to determine the hydrogenlike ionization cross section.

(Charge exchange between a highly charged ion and another ion such as Ne^{1+} is negligible at the low kinetic energies of the ions in our trap because Coulomb repulsion limits the distance of closest approach.) We used the evaporative cooling effect of neutral background gas to confirm that the background gas density was small. The absolute RR($n=1$) x-ray count rate (measured relative to a repetitive pulser) was recorded at different neon densities, as shown in Fig. 4. At low densities the count rate is expected to have a nearly linear dependence on gas density, becoming zero at zero neon density. The measured count rate behaves as expected, indicating that the density of background gas in the trap is small.

4. Modified extrapolation for heavy elements

For the heavier elements (dysprosium, gold, and bismuth), the RR(bare) count rate is too low to be used in a determination of the correction for charge-exchange recombination. Instead we determined the rate of charge exchange from the ratio of two much stronger RR lines: the (blended) L-shell RR line and the K-shell RR line from hydrogenlike target ions. A correction for the energy dependence of the detector efficiency was included in the calculation of this ratio. For gold and bismuth only the $J=1/2$ component of the L-shell RR was used. Although several charge states contribute to RR into $n=2$ orbitals, the shift in ionization balance caused by charge-exchange recombination is expected to produce a nearly linear relationship, similar to Eq. (8), between the ratio $I^{\mathrm{RR}}_{n=2}/I^{\mathrm{RR}}_{\mathrm{H}}$ and the neutral neon density. Measurements of this ratio and the number of trapped bismuth ions are shown in Fig. 5. Here the strong RR($n=3$) line was used as a measure of the number of bismuth ions, which is appropriate because the M shell is completely vacant for all of the bismuth charge states present in the trap.

The following procedure was used to determine $\langle \sigma^{\mathrm{CX}}_{\mathrm{bare}} \rangle$ for bare ions of dysprosium, gold, and bismuth. First, the ratio $I^{\mathrm{RR}}_{n=2}/I^{\mathrm{RR}}_{\mathrm{H}}$ was extrapolated to zero neutral density (the broken line in Fig. 5), at which point there is no charge-exchange recombination. Next, calculated RR cross sections, and relative ionization cross sections for the different charge states obtained from the Lotz formula [19], were used to search for a normalization factor for the Lotz ionization cross sections that yields an ionization balance with the correct

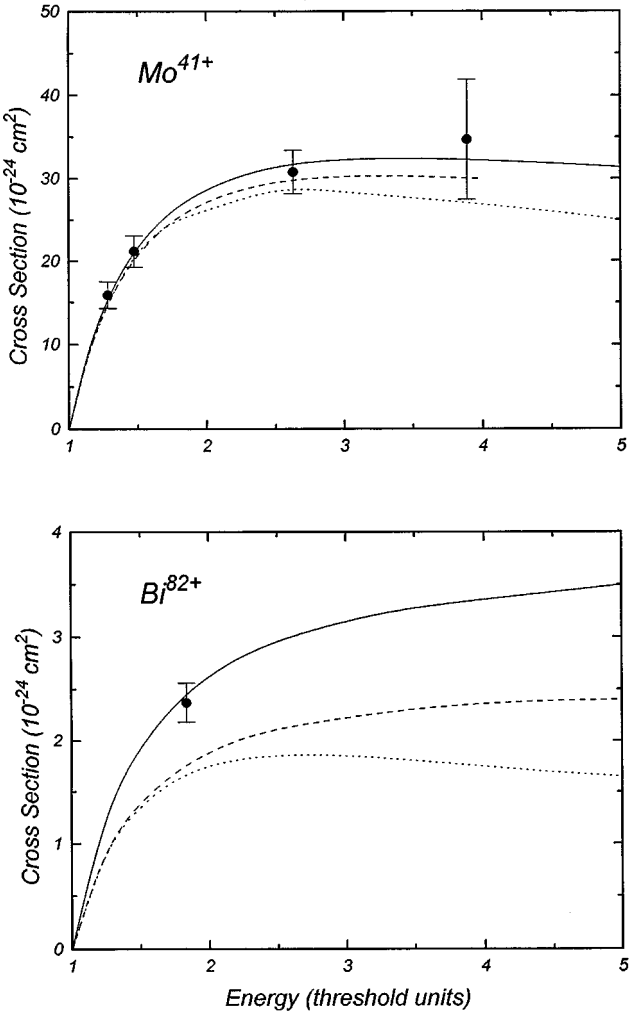

FIG. 6. The measured ionization cross sections for hydrogenlike molybdenum and bismuth compared to the relativistic distorted wave calculations of Ref. [4]. Solid curve: complete calculation including the Moeller interaction. Dashed curve: relativistic calculation with the Coulomb interaction only. Dotted curve: nonrelativistic calculation.

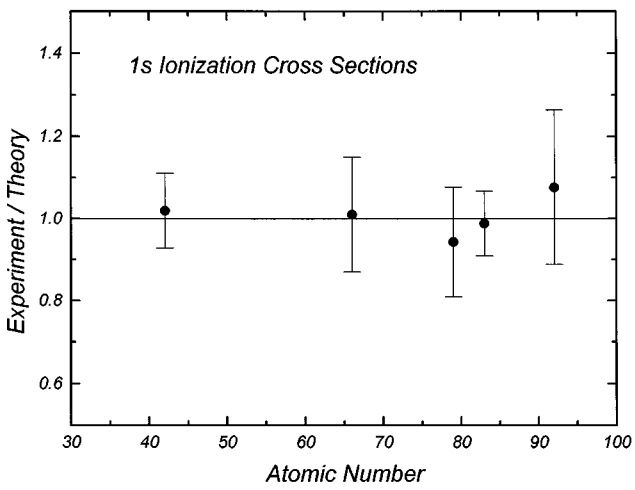

FIG. 7. Comparison of experiment and relativistic distorted wave theory with the Moeller interaction (Ref. [4]) for hydrogenlike ions at $E_e \approx 1.5$ threshold units. (See Table I for exact energy values.)

extrapolated (i.e., no charge exchange) $I^{\mathrm{RR}}_{n=2}/I^{\mathrm{RR}}_{\mathrm{H}}$ ratio. Finally, with the normalized ionization cross sections held fixed in the search procedure, a sufficient amount of charge exchange was included to reproduce the observed $I^{\mathrm{RR}}_{n=2}/I^{\mathrm{RR}}_{\mathrm{H}}$ ratio at nonzero neon density. The charge-exchange recombination cross section for the different ions was assumed to be proportional to the ion charge as suggested by other measurements [20,21], and was assumed to be dominated by single charge exchange, so only one overall charge-exchange factor was adjusted to match the observed $I^{\mathrm{RR}}_{n=2}/I^{\mathrm{RR}}_{\mathrm{H}}$ intensity ratio.

This procedure determines the value of $\langle \sigma^{\mathrm{CX}}_{\mathrm{bare}} \rangle$ as a function of neon density and allows $\sigma^{\mathrm{ion}}_{\mathrm{H}\rightarrow\mathrm{bare}}$ to be determined from Eq. (7). Hydrogenlike ionization cross sections for each element were determined from long runs at an intermediate neon density. (For bismuth this corresponds to the point with the small error bar in Fig. 5.) Although the adjustment of the theoretical (Lotz) ionization cross sections to match the extrapolated (no charge exchange) ratio of RR intensities does provide information on the size of the ionization cross sections for L-shell and K-shell electrons, we do not use it for this purpose. The adjusted Lotz ionization cross sections are used only for estimating the charge-exchange recombination rate. The value of $\langle \sigma^{\mathrm{CX}}_{\mathrm{bare}} \rangle$ obtained is relatively insensitive to the details of the above procedure, such as the assumed relative size of the ionization cross sections for the different ion charge states. We conservatively estimate the error in $\langle \sigma^{\mathrm{CX}}_{\mathrm{bare}} \rangle$ to be 50% of its value. Although this uncertainty is large, it translates into a much smaller percentage error contribution to the ionization cross section because recombination is dominated by RR [see Eq. (7) and Table I].

III. IONIZATION CROSS SECTIONS

Our measured ionization cross sections for hydrogenlike ions are listed in Table I. They were obtained from Eq. (7) as described above. The listed uncertainties are the quadrature sum of the statistical uncertainties, an assumed 50% uncertainty in the correction for charge-exchange recombination, and an estimated 2% additional systematic error from the line-shape fitting. The estimated 3% uncertainty in the RR cross sections used for normalization is not included.

There have been numerous theoretical calculations of electron-impact ionization cross sections. The most relevant for the present work are those by Moores and Reed [4] and those by Fontes, Sampson, and Zhang [3]. Both of these groups explored the effects of first order QED (i.e., the Breit or Moeller interaction) and exchange terms in relativistic distorted wave calculations. Both groups found that the exchange terms are important, and that inclusion of the Moeller interaction, as opposed to the static Coulomb interaction, significantly increases the ionization cross section at higher electron energy.

Calculations for the same elements studied in the present work have been reported in Ref. [4], and we include those results (with and without the Moeller interaction) in Table I. In all cases our measurements agree with relativistic distorted wave theory that includes both exchange and the Moeller interaction. The measurements disagree with calcu-

lations that include only the Coulomb interaction at higher electron energies where these calculations diverge from those with the Moeller interaction. The energy dependence of the ionization cross sections for molybdenum and bismuth are shown in Fig. 6.

A convenient semiempirical formula due to Lotz is widely used to estimate electron-impact ionization cross sections [19]. For hydrogenlike ions it has the form

$$\sigma_{\mathrm{H}}^{\mathrm{ion}}(\mathrm{Lotz}) = 4.5\times 10^{-14}\,\frac{\ln(E_e/I_{\mathrm{H}})}{E_e I_{\mathrm{H}}} \quad (\mathrm{cm}^2), \tag{9}$$

where E_e is the incident electron energy and I_{H} is the ionization potential of the hydrogenlike target ion in eV. Lotz-formula cross sections are given in the last column of Table I. It can be seen that the Lotz formula systematically underestimates the true cross sections, particularly at the highest electron energies, where it is too low by as much as a factor of two.

At least one electron energy at which cross sections were measured is very close to 1.5 in threshold units for each element studied, enabling a study of the Z dependence of the ionization cross sections at (nearly) constant energy in threshold units. This is displayed graphically in Fig. 7, where the ratios of the experimental and theoretical (relativistic distorted wave with the Moeller interaction) cross sections are plotted. The excellent agreement between theory and experiment for a wide range of atomic number and electron energy suggests that electron-impact ionization for K-shell electrons is now sufficiently well understood to determine reliable cross sections for all heavy elements.

ACKNOWLEDGMENTS

We thank K. J. Reed for helpful discussions and for providing theoretical ionization cross sections. This work was supported in part by the Office of Basic Energy Sciences, Division of Chemical Sciences, U.S. Department of Energy, and was performed under the auspices of the U.S. Department of Energy by the Lawrence Livermore National Laboratory under Contract No. W-7405-Eng-48.

[1] H. L. Zhang and D. H. Sampson, Phys. Rev. A **42**, 5378 (1990).
[2] D. L. Moores and M. S. Pindzola, Phys. Rev. A **41**, 3603 (1990).
[3] C. J. Fontes, D. H. Sampson, and H. L. Zhang, Phys. Rev. A **51**, R12 (1995).
[4] D. L. Moores and K. J. Reed, Nucl. Instrum. Methods Phys. Res. B **98**, 122 (1995); Phys. Rev. A **51**, R9 (1995).
[5] R. E. Marrs, S. R. Elliott, and D. A. Knapp, Phys. Rev. Lett. **72**, 4082 (1994).
[6] J. Linkemann, A. Müller, J. Kenntner, D. Habs, D. Schwalm, A. Wolf, N. R. Badnell, and M. S. Pindzola, Phys. Rev. Lett. **74**, 4173 (1995).
[7] D. C. Gregory, L. J. Wang, D. R. Swenson, M. Sataka, and S. J. Chantrenne, Phys. Rev. A **41**, 6512 (1990).
[8] E. D. Donets, in *The Physics and Technology of Ion Sources*, edited by I. G. Brown (John Wiley, New York, 1989), p. 245.
[9] K. L. Wong, P. Beiersdorfer, M. H. Chen, R. E. Marrs, K. J. Reed, J. H. Scofield, D. A. Vogel, and R. Zasadzinski, Phys. Rev. A **48**, 2850 (1993).
[10] N. Claytor, B. Feinberg, H. Gould, C. E. Bemis, J. G. Campo, C. A. Ludemann, and C. R. Vane, Phys. Rev. Lett. **61**, 2081 (1988).
[11] D. A. Knapp, R. E. Marrs, S. R. Elliott, E. W. Magee, and R. Zasadzinski, Nucl. Instrum. Methods Phys. Res. A **334**, 305 (1993).
[12] J. H. Scofield, Phys. Rev. A **40**, 3054 (1989).
[13] E. B. Saloman, J. H. Hubbell, and J. H. Scofield, At. Data Nucl. Data Tables **38**, 1 (1988).
[14] R. H. Pratt, A. Ron, and H. K. Tseng, Rev. Mod. Phys. **45**, 273 (1973).
[15] R. E. Marrs, M. A. Levine, D. A. Knapp, and J. R. Henderson, Phys. Rev. Lett. **60**, 1715 (1988).
[16] R. E. Marrs, in *Experimental Methods in the Physical Sciences Volume 29A*, edited by F. B. Dunning and R. G. Hulet (Academic Press, San Diego, 1995), p. 391.
[17] M. A. Levine, R. E. Marrs, J. R. Henderson, D. A. Knapp, and M. B. Schneider, Phys. Scr. **T22**, 157 (1988).
[18] I. G. Brown, J. E. Galvin, R. A. MacGill, and R. T. Wright, Appl. Phys. Lett. **49**, 1019 (1986).
[19] W. Lotz, Z. Phys. **216**, 241 (1968).
[20] A. Müller and E. Salzborn, Phys. Lett. **62A**, 391 (1977).
[21] B. R. Beck, J. Steiger, G. Weinberg, D. A. Church, J. McDonald, and D. Schneider, Phys. Rev. Lett. **77**, 1735 (1996).